

**Graphene quantum dot with a Coulomb impurity: Subcritical and supercritical regime**R. Van Pottelberge,<sup>1,\*</sup> M. Zarenia,<sup>1,†</sup> P. Vasilopoulos,<sup>2,‡</sup> and F. M. Peeters<sup>1,§</sup><sup>1</sup>*Departement Fysica, Universiteit Antwerpen Groenenborgerlaan 171, B-2020 Antwerpen, Belgium*<sup>2</sup>*Department of Physics, Concordia University, Montreal, Quebec, Canada H4B 1R6*

(Received 10 March 2017; revised manuscript received 8 May 2017; published 12 June 2017)

We study the influence of confinement on the atomic collapse due to a Coulomb impurity placed at the center of a graphene quantum dot of radius  $R$ . We apply the zigzag or infinite-mass boundary condition and consider both a point-size and a finite-size impurity. As a function of the impurity strength  $Z\alpha$ , the energy spectra are discrete. In the case of the zigzag boundary condition, the degenerate (with respect to the angular momentum  $m$ ) zero-energy levels are pulled down in energy as  $Z\alpha$  increases, and they remain below  $\epsilon = -Z\alpha$ . Our results show that the energy levels exhibit a  $1/R$  dependence in the subcritical regime [ $Z\alpha < |km + 1/2|$ ,  $k = 1$  ( $-1$ ) for the  $K$  ( $K'$ ) valley]. In the supercritical regime ( $Z\alpha > |km + 1/2|$ ) we find a qualitatively very different behavior where the levels decrease as a function of  $R$  in a nonmonotonic manner. While the valley symmetry is preserved in the presence of the impurity, we find that the impurity breaks electron-hole symmetry. We further study the energy spectrum of zigzag quantum dots in gapped graphene. Our results show that as the gap increases, the lowest electron states are pushed into the gap by the impurity.

DOI: [10.1103/PhysRevB.95.245410](https://doi.org/10.1103/PhysRevB.95.245410)**I. INTRODUCTION**

The atomic collapse with heavy nuclei, having a large atomic number  $Z$ , is a well-studied problem in quantum electrodynamics (QED). Solving the Dirac equation for an atomic nucleus, treated as a point charge, gives the energy of the  $1S$  atomic bound state,  $E_{1S} = m_e[1 - (Z\alpha)^2]^{1/2}$ , where  $m_e \approx 511$  keV is the electron rest mass and  $\alpha \approx 1/137$  is the fine-structure constant [1]. Beyond  $Z_c\alpha = 1$ , i.e.,  $Z_c \approx 137$ , the energy of the  $1S$  state becomes imaginary. This collapses the wave function and the bound state ceases to exist. However, taking into account the finite size of the nucleus truncates the Coulomb potential and removes the divergence. This extends the stability of the  $1S$  state up to a new critical value  $Z_c \approx 170$  [1,2]. The range of stability  $Z < Z_c$  is referred to as the *subcritical* regime and that for  $Z > Z_c$  as the *supercritical* regime. In the latter, the electron state leaves the discrete spectrum and tunnels into the positron continuum. That is, the bound state acquires a finite lifetime and becomes a narrow resonance [1,3]. This is referred to as the *atomic collapse*. A stable nucleus with  $Z > 170$ , not found in nature, is possible to realize, for a very short time, in high-energy collisions of very heavy ions, but experiments with uranium atoms provided no direct proof of the expected supercritical positron emission [4].

The difficulties mentioned above can be drastically alleviated in graphene in which the charge carriers (electrons) are massless and exhibit relativistic behavior with the speed of light replaced by the much smaller Fermi velocity  $v_F \approx c/300$ . This leads to the same atomic collapse physics of QED but at a much smaller energy scale and in two dimensions. The effective fine-structure constant becomes  $\alpha_g = c/v_F\kappa \approx 2.2/\kappa \approx 1$ , where  $\kappa \approx 2.5$  is the dielectric constant of graphene [5] with its three-dimensional (3D) environment. Correspondingly, the critical charge  $Z_c$  is expected to

be much smaller, i.e., of the order of unity, and the energy scale changes from MeV to sub-eV. Accordingly, charged impurities in graphene could play the role of supercritical nuclei [6,7]. The recent observations of the expected resonances around artificial nuclei [8] and the realization of tunable artificial atoms at supercritically charged vacancies [9] in extended graphene sheets confirmed the analog of the QED atomic collapse and gave new impetus for further studies. Given that graphene is experimentally accessible, one can further study this analog of the atomic collapse by varying other parameters such as back-gate voltage, defects, the influence of a magnetic field, etc., and better understand confinement in graphene.

Motivated by these results on bulk graphene, we study the influence of confinement on the atomic collapse by placing a Coulomb impurity in a gapped or gapless graphene quantum dot (QD), and we investigate how the usual bound states induced by the dot are modified upon varying the impurity strength. QDs in graphene have been the subject of a considerable number of theoretical and experimental studies [10–12]. QDs in monolayer graphene (MLG) have been fabricated by direct etching of pristine graphene sheets into small flakes [12]. In these structures, the shape and edges of the sample can strongly influence the confined states [13]. The electronic and transport properties of such QDs with different shapes and edges have been investigated extensively [14–18].

Here we analytically solve the Dirac-Weyl equation for a circular graphene QD in the presence of a Coulomb impurity at its center. We consider QDs with both zigzag (ZZBCs) and infinite-mass (IMBCs) boundary conditions. We notice that a circular QD cut out of graphene has both armchair and zigzag edges. However, in order to obtain analytical results for the energy levels and to observe features brought about by the zigzag edges in the spectrum, we enforce the zigzag boundary condition. We further investigate the influence of a mass potential on the spectrum with a ZZBC. We first treat the Coulomb impurity as a *point-size* charge that gives solutions only in the *subcritical* regime. Considering a *finite-size* impurity (of the order of graphene's lattice constant), we obtain solutions in both the subcritical and supercritical regimes.

\*robbe.vanpottelberge@student.uantwerpen.be

†mohammad.zarenia@uantwerpen.be

‡p.vasilopoulos@concordia.ca

§francois.peeters@uantwerpen.be

The paper is organized as follows. In Sec. II we present some general results for a dot without a Coulomb impurity and for different boundary conditions. In Sec. III we present our model of a point-size Coulomb impurity in the subcritical regime and in Sec. IV that of a finite-size impurity in the supercritical regime. The corresponding numerical results are presented in Sec. V and our summary is given in Sec. VI.

## II. CIRCULAR QUANTUM DOTS IN GRAPHENE

The general problem that we want to solve consists of a quantum dot in gapped graphene in the presence of a Coulomb impurity. The corresponding Hamiltonian is given by

$$H = -i\hbar v_F \left( k\sigma_1 \frac{\partial}{\partial x} + \sigma_2 \frac{\partial}{\partial y} \right) + \Delta\sigma_3 + IV(r). \quad (1)$$

Here  $\sigma_i$ ,  $i = 1, 2, 3$ , are the Pauli matrices,  $V(r) = -Z\alpha/r$  is the impurity potential,  $Z$  is the atomic number,  $\alpha = e^2/4\pi\epsilon_0$ , and  $k = 1$  ( $-1$ ) denotes, respectively, the  $K$  and  $K'$  valleys. Further,  $v_F$  is the Fermi velocity,  $\Delta = m_{\text{eff}}v_F^2$  is the band gap, and  $I$  is the  $2 \times 2$  identity matrix. The eigenvalues  $E$  and eigenfunctions  $\Psi$  are obtained from Schrödinger's equation  $H\Psi = E\Psi$ . The two-component eigenfunctions are written in the form  $\Psi = (\psi_a, \psi_b)^T$ , with  $T$  denoting the transpose, due to the two sublattices of graphene.

We consider a circular quantum dot, of radius  $R$ , in line with the radial symmetry of  $V(r)$ . The impurity is placed at the origin. Further, we introduce the dimensionless variables  $\rho = r/R$ ,  $\epsilon = ER/\hbar v_F$ ,  $\delta = \Delta R/\hbar v_F$ , and  $\alpha = \alpha_0/\hbar v_F$ . Then Eq. (1) leads to a set of coupled equations for the components  $\psi_a, \psi_b$ , namely

$$\left( \epsilon - \delta + \frac{Z\alpha}{\rho} \right) \psi_a + e^{-ik\theta} \left( ik \frac{\partial}{\partial \rho} + \frac{1}{\rho} \frac{\partial}{\partial \theta} \right) \psi_b = 0, \quad (2a)$$

$$\left( \epsilon + \delta + \frac{Z\alpha}{\rho} \right) \psi_b + e^{ik\theta} \left( ik \frac{\partial}{\partial \rho} - \frac{1}{\rho} \frac{\partial}{\partial \theta} \right) \psi_a = 0. \quad (2b)$$

### A. Boundary conditions

Before solving the coupled set of Eqs. (2a) and (2b), it is very important to specify the proper boundary conditions. To do so, we know that for the Dirac Hamiltonian (1) the electron current at a point  $\rho$  is given by

$$\begin{aligned} \mathbf{j}(\rho, \theta) &= (\psi_a^*, \psi_b^*) (\sigma_x, \sigma_y) \begin{pmatrix} \psi_a \\ \psi_b \end{pmatrix} \\ &= 2(\text{Re}[\psi_a^*(\rho, \theta)\psi_b(\rho, \theta)], \text{Im}[\psi_a^*(\rho, \theta)\psi_b(\rho, \theta)])^T. \end{aligned} \quad (3)$$

At the edge of the dot, we have  $\rho = 1$  and the outward electron current vanishes since electrons are confined inside the dot. This condition can be written in terms of the normal  $\mathbf{n}(\theta)$  at the dot's edge,  $\mathbf{n}(\theta) = (\cos \theta, \sin \theta)^T$ , shown in Fig. 1. Note that  $\mathbf{n}$  depends *only* on the angle  $\theta$ . This is valid only for a circular quantum dot. For a dot of another shape, this normal will depend on the particular value of  $\rho$  at its edge.

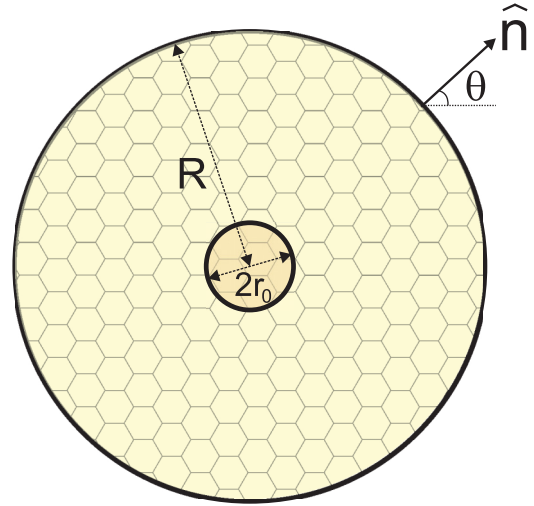


FIG. 1. Schematics of a circular dot, of radius  $R$ , with an impurity of radius  $r_0$  at the origin.

The boundary condition that the outward electron current vanishes at the dot edge ( $\rho = 1$ ) takes the form

$$\mathbf{j}(1, \theta) \cdot \mathbf{n}(\theta) = 0. \quad (4)$$

Using Eq. (3), this condition becomes

$$\cos \theta \text{Re}[\psi_a^*(1, \theta)\psi_b(1, \theta)] + \sin \theta \text{Im}[\psi_a^*(1, \theta)\psi_b(1, \theta)] = 0. \quad (5)$$

Equation (5) is satisfied for

$$\psi_a(1, \theta) = 0 \text{ or } \psi_b(1, \theta) = 0. \quad (6)$$

Equation (6) is called the ZZBC and corresponds physically to a boundary with all missing carbon atoms belonging to the same sublattice.

Equation (5) is also satisfied for [19]

$$\psi_b(1, \theta) = iC e^{i\theta} \psi_a(1, \theta), \quad (7)$$

where  $C$  is a constant. To clearly see how this corresponds to a physical situation, we assume gapless graphene and replace  $\Delta$  by a masslike potential  $M(r)$  in Eq. (1). The value  $C = 1$  corresponds to the case  $M(r) = 0$  inside the dot and  $M(r) \rightarrow \infty$  outside it. Equation (7) is called the IMBC, as was originally proposed in Ref. [19]. The region outside the dot is forbidden for electrons because they have then an infinite mass. This holds for the  $K$  valley. For the  $K'$  valley, we have  $C = -1$  with  $M(r) = 0$  inside the dot and  $M(r) \rightarrow -\infty$  outside it. Thus, the IMBC distinguishes between the  $K$  and  $K'$  valleys. Experimental realization of IMBC in graphene is challenging. However, one can use graphene on top of a hexagonal boron nitride (h-BN) substrate, which induces a staggered potential in graphene that breaks the sublattice symmetry and opens an energy gap [20–22].

### B. Quantum dot states

The energy levels of circular graphene QDs in the absence of a Coulomb impurity ( $Z\alpha = 0$ ) have been studied in Ref. [16] even in the presence of a perpendicular magnetic field. However, it is helpful to recall the wave functions and some aspects of the energy levels in the case of zero magnetic field.

Considering solutions with azimuthal symmetry, we attempt them in the form  $\psi_a = R_a(\rho)e^{im\theta}$ , where the angular momentum  $m$  can take the values  $0, \pm 1, \pm 2, \dots$ . Then Eqs. (2a) and (2b) take a simpler form. For  $|\epsilon| > \delta$ , the solutions of Eq. (2a) are the Bessel functions  $J_m(\epsilon_\delta \rho)$  with  $\epsilon_\delta = (\epsilon^2 - \delta^2)^{1/2}$ , so that  $\psi_a = e^{im\theta} J_m(\epsilon_\delta \rho)$ , and using Eq. (2b) we find  $\psi_b$ . The end results for  $\psi_a$  and  $\psi_b$  are

$$\psi_a = N\sqrt{|\epsilon + \delta|}e^{im\theta} J_m(\epsilon_\delta \rho), \quad (8a)$$

$$\psi_b = \pm Ni\sqrt{|\epsilon - \delta|}e^{i(m+k)\theta} J_{m+k}(\epsilon_\delta \rho), \quad (8b)$$

where  $N$  is a normalization constant. The  $+$  sign is for  $\epsilon > \delta > 0$  and the  $-$  sign for  $\epsilon < -\delta$ . Notice that the total angular momentum operator  $J_z$  in graphene is given by the sum of the orbital angular momentum  $L_z$  and a term describing the pseudospin  $J_z = L_z + (\hbar/2)\sigma_3$ , so that the eigenvalues of  $J_z$  become  $m + \hbar/2$ .

Following the same procedure for  $|\epsilon| < \delta$ , the final solutions are

$$\psi_a = N\sqrt{\epsilon + \delta}e^{im\theta} I_m(-i\epsilon_\delta \rho), \quad (9a)$$

$$\psi_b = -Nik\sqrt{\delta - \epsilon}e^{i(m+k)\theta} I_{m+k}(-i\epsilon_\delta \rho). \quad (9b)$$

Here  $I_m$  denotes the modified Bessel function of order  $m$ . When the gap vanishes, Eqs. (8a) and (8b) become

$$\psi_a = N\sqrt{|\epsilon|}e^{im\theta} J_m(\epsilon\rho), \quad \psi_b = Ni\sqrt{|\epsilon|}e^{i(m+k)\theta} J_{m+k}(\epsilon\rho). \quad (10)$$

For QDs with the ZZBC, the solutions are bound only for  $|\epsilon| > \delta$  and the energy levels can be determined from  $\psi_a(1, \theta) = 0$  or  $\psi_b(1, \theta) = 0$ , given in Eqs. (8a) and (8b), depending on which atoms are at the edge of the dot [23]. This gives

$$J_m(\epsilon_\delta) = 0 \quad \text{or} \quad J_{m+k}(\epsilon_\delta) = 0. \quad (11)$$

A few properties can be deduced from Eq. (11) using those of the Bessel functions [24]. The intravalley symmetries for electron ( $e$ ) and hole ( $h$ ) states are

$$\epsilon_{\pm 1, a, m}^{e, h} = \epsilon_{\pm 1, a, -m}^{e, h}, \quad (12a)$$

$$\epsilon_{\pm 1, i, m}^e = -\epsilon_{\pm 1, i, m}^h, \quad i = a, b, \quad (12b)$$

Here,  $+1$  ( $-1$ ) denotes the  $K$  ( $K'$ ) valley, and  $a$  ( $b$ ) refers to sublattice  $\psi_a = 0$  ( $\psi_b = 0$ ) at the edge of the dot. We emphasize that the spectra obtained from  $\psi_a(1, \theta) = 0$  and  $\psi_b(1, \theta) = 0$  are exactly the same except that the  $m$  value is shifted by  $\pm 1$ , i.e.,

$$\epsilon_{\pm 1, a, m}^{e, h} = \epsilon_{\pm 1, b, -(m\pm 1)}^{e, h}, \quad (13)$$

and for nonzero  $\delta$ , the condition  $\psi_a(1, \theta) = 0$  gives degenerate states with  $\epsilon = -\delta$  (for  $m < 0$ ) and  $\psi_b(1, \theta) = 0$  gives degenerate states with  $\epsilon = \delta$  (for  $m \geq 0$ ).

The connection between the valleys is described by

$$\epsilon_{+1, i, m}^{e, h} = \epsilon_{-1, i, -m}^{e, h}, \quad i = a, b, \quad (14)$$

and it will become more clear later in this paper. The spectra for the  $K$  and  $K'$  valleys are exactly the same, which can be seen from Eq. (14).

Applying the IMBC (7) to the solutions (10) leads to  $J_{m+1}(\epsilon) = \tau J_m(\epsilon)$ , where  $\tau$  distinguishes between the two valleys. Solving this equation will give the IMBC spectrum. In the case of the ZZBC, we found that there are zero-energy degenerate edge states [16]. This is not the case for the IMBC in which the electron-hole, Eq. (12a), and intervalley, Eq. (14), relations are not valid anymore. However, there are other relations that can be derived [16],

$$\epsilon_{\pm 1, m}^e = -\epsilon_{\pm 1, -(m+1)}^h, \quad (15a)$$

$$\epsilon_{1, m}^{e, h} = \epsilon_{-1, -(m+1)}^{e, h}. \quad (15b)$$

### III. ZERO-SIZE IMPURITY: SUBCRITICAL REGIME

We consider the case of a Coulomb impurity placed at the center of the QD. Using the Hamiltonian (1), we obtain analytical expressions for the wave functions for both zero- and finite-mass term potential  $\delta$ . We then apply the ZZBC for  $\delta = 0$  and  $\delta \neq 0$ . The IMBC is applied only to the case  $\delta = 0$ .

Using Eqs. (2a) and (2b) and considering the solutions

$$\psi_a = e^{im\theta} R_a(\rho), \quad \psi_b = ik e^{i(m+k)\theta} R_b(\rho), \quad (16)$$

with  $m$  being the angular momentum label, we obtain

$$\left(\frac{\partial}{\partial \rho} + \frac{mk+1}{\rho}\right)R_b(\rho) - \left(\epsilon - \delta + \frac{Z\alpha}{\rho}\right)R_a(\rho) = 0, \quad (17)$$

$$\left(\frac{\partial}{\partial \rho} - \frac{km}{\rho}\right)R_a(\rho) + \left(\epsilon + \delta + \frac{Z\alpha}{\rho}\right)R_b(\rho) = 0. \quad (18)$$

The key now is to decouple these equations. We discuss two possible energy regimes:  $|\epsilon| < \delta$  and  $|\epsilon| > \delta$ .

(i)  $|\epsilon| < \delta$ . The equations can be decoupled using the ansatz [25]

$$\begin{pmatrix} \psi_a \\ \psi_b \end{pmatrix} = e^{im\theta - \frac{\nu}{2}} \rho_*^{\nu-1/2} \begin{pmatrix} \sqrt{\delta + \epsilon} (P + Q) \\ ik e^{i\theta} \sqrt{\delta - \epsilon} (P - Q) \end{pmatrix}, \quad (19)$$

where  $\rho_* = 2\gamma\rho$ ,  $\nu = [(km + 1/2)^2 - (Z\alpha)^2]^{1/2}$ , and  $\gamma = [\delta^2 - \epsilon^2]^{1/2}$ . Then setting  $\omega_\gamma = Z\alpha\epsilon/\gamma$ , the resulting equations for  $P$  and  $Q$  are of the form

$$x \frac{\partial^2 f(x)}{\partial \rho_*^2} + (b-x) \frac{\partial f(x)}{\partial \rho_*} - af(x) = 0; \quad (20)$$

here  $b = 1 + 2\nu$  for  $P$  and  $Q$ , while  $a = \nu - \omega_\gamma$  for  $P$  and  $a = 1 + \nu - \omega_\gamma$  for  $Q$ .

Equation (20) has two linear independent solutions, namely the hypergeometric functions

$${}_1F_1(a, b, x), \quad x^{1-b} {}_1F_1(a-b+1, 2-b, x). \quad (21)$$

The solution  $x^{1-b} {}_1F_1(a-b+1, 2-b, x)$  is singular at the origin for  $b$  real and will be discarded. Accordingly, the solutions for  $P$  and  $Q$  are

$$P(\rho_*) = A {}_1F_1(\nu - \omega_\gamma, 1 + 2\nu, \rho_*), \quad (22a)$$

$$Q(\rho_*) = B {}_1F_1(1 + \nu - \omega_\gamma, 1 + 2\nu, \rho_*). \quad (22b)$$

It can be shown that the constants  $A$  and  $B$  are related [26],

$$\frac{A}{B} = \frac{j + \eta_\gamma}{\nu - \omega_\gamma} = \frac{\nu + \omega_\gamma}{j - \eta_\gamma}, \quad (23)$$

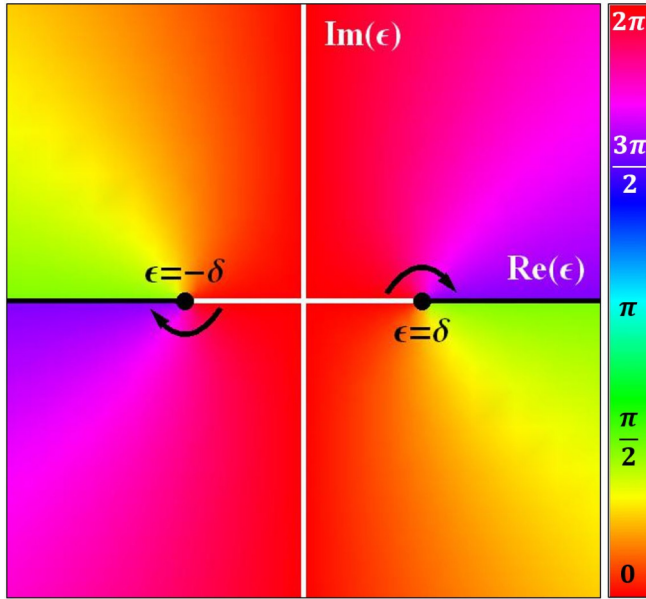


FIG. 2. Analytic continuation in the energy domain. Note that only the phase is shown.

where  $j = km + 1/2$  and  $\eta_\gamma = Z\alpha\delta/\gamma$ . Using Eq. (23) and the exact form of  $P$  and  $Q$ , we can determine the wave functions

$$\begin{aligned} \psi_a &= N\sqrt{\delta + \epsilon} e^{i(j-1/2)\theta} e^{-\gamma\rho} (2\gamma\rho)^{\nu-1/2} \\ &\times [(j + \eta_\gamma)_1 F_1(\nu - \omega_\gamma, 1 + 2\nu, 2\gamma\rho) \\ &+ (\nu - \omega_\gamma)_1 F_1(1 + \nu - \omega_\gamma, 1 + 2\nu, 2\gamma\rho)], \end{aligned} \quad (24a)$$

$$\begin{aligned} \psi_b &= ikN\sqrt{\delta - \epsilon} e^{i(j+1/2)\theta} e^{-\gamma\rho} (2\gamma\rho)^{\nu-1/2} \\ &\times [(j + \eta_\gamma)_1 F_1(\nu - \omega_\gamma, 1 + 2\nu, 2\gamma\rho) \\ &- (\nu - \omega_\gamma)_1 F_1(1 + \nu - \omega_\gamma, 1 + 2\nu, 2\gamma\rho)]. \end{aligned} \quad (24b)$$

$N$  is a normalization constant, and  $j = \pm 1/2, \pm 3/2, \dots$ . Note that the above solutions are valid only for  $\nu$  real (i.e.,  $Z\alpha \leq |j|$ ). The onset value of  $Z\alpha$ , for which  $\nu$  becomes imaginary, is obtained by setting  $j = \pm 1/2$ . Accordingly, we enter the supercritical regime for  $Z\alpha > 1/2$ .

Applying the ZZBC to the solutions (24a) and (24b) gives the following equations, respectively, for  $\psi_a(1, \theta) = 0$  and  $\psi_b(1, \theta) = 0$ :

$$(j + \eta_\gamma)_1 F_1(\nu - \omega_\gamma, 1 + 2\nu, 2\gamma) + (\nu - \omega_\gamma)_1 F_1(1 + \nu - \omega_\gamma, 1 + 2\nu, 2\gamma) = 0, \quad (25a)$$

$$(j + \eta_\gamma)_1 F_1(\nu - \omega_\gamma, 1 + 2\nu, 2\gamma) - (\nu - \omega_\gamma)_1 F_1(1 + \nu - \omega_\gamma, 1 + 2\nu, 2\gamma) = 0. \quad (25b)$$

The roots of these equations give the energy spectrum.

(ii)  $|\epsilon| > \delta$ . This pertains to energies above the band gap. Without confinement, the spectrum is continuous. Due to the confinement by the QD, it becomes discrete. To determine the wave functions and then the spectrum via the ZZBC and IMBC, we perform an analytic continuation in the energy domain [26]. Consider the complex plane of  $\epsilon$  (see Fig. 2) with the branch cuts along the real axis connecting the points

$\epsilon = \pm\delta$  with infinity. The states on the branch cuts correspond to the continuous spectrum, while the real poles in the interval  $-\delta < \epsilon < \delta$  correspond to bound states.

Explicitly, the analytic continuation is embodied in the relations

$$\sqrt{\delta - \epsilon} \rightarrow -i\sqrt{|\epsilon - \delta|}, \quad \sqrt{\delta + \epsilon} \rightarrow \sqrt{|\epsilon + \delta|}, \quad \epsilon > \delta, \quad (26a)$$

$$\sqrt{\delta - \epsilon} \rightarrow \sqrt{|\epsilon - \delta|}, \quad \sqrt{\delta + \epsilon} \rightarrow -i\sqrt{|\epsilon + \delta|}, \quad \epsilon < -\delta. \quad (26b)$$

Applying these transformations to Eqs. (24a) and (24b) gives the wave functions

$$\begin{aligned} \psi_a &= N'\sqrt{|\delta + \epsilon|} e^{i(j-1/2)\theta} e^{i\beta\rho} \rho^{\nu-1/2} \\ &\times [(j + i\eta_\beta)_1 F_1(\nu - i\omega_\beta, 1 + 2\nu, -2i\beta\rho) \\ &+ (\nu - i\omega_\beta)_1 F_1(1 + \nu - i\omega_\beta, 1 + 2\nu, -2i\beta\rho)], \end{aligned} \quad (27a)$$

$$\begin{aligned} \psi_b &= \pm kN'\sqrt{|\epsilon - \delta|} e^{i(j-1/2)\theta} e^{i\beta\rho} \rho^{\nu-1/2} \\ &\times [(j + i\eta_\beta)_1 F_1(\nu - i\omega_\beta, 1 + 2\nu, -2i\beta\rho) \\ &- (\nu - i\omega_\beta)_1 F_1(1 + \nu - i\omega_\beta, 1 + 2\nu, -2i\beta\rho)], \end{aligned} \quad (27b)$$

where  $\beta = [\epsilon^2 - \delta^2]^{1/2}$ ,  $\omega_\beta$  is given by  $Z\alpha\epsilon/\beta$ , and  $N' = N(2i\beta)^{\nu-1/2}$ . The  $+$  ( $-$ ) sign is for  $\epsilon > \delta$  ( $\epsilon < -\delta$ ).

Applying the ZZBC to the above solutions leads to Eqs. (25a) and (25b) with the changes  $\gamma \rightarrow -i\beta$ ,  $\eta_\gamma \rightarrow i\eta_\beta$ , and  $\omega_\gamma \rightarrow i\omega_\beta$ .

(iii)  $\delta = 0$ . This is the case of gapless graphene. The wave functions can be simply obtained by putting  $\delta = 0$  in Eqs. (27a) and (27b). The results are

$$\begin{aligned} \psi_a &= N' e^{i(j-\frac{1}{2})\theta} e^{i|\epsilon|\rho} \rho^{\nu-\frac{1}{2}} \\ &\times [j_1 F_1(\nu - \bar{Z}, 1 + 2\nu, -2i|\epsilon|\rho) + (\nu - \bar{Z}) \\ &\times {}_1F_1(1 + \nu - \bar{Z}, 1 + 2\nu, -2i|\epsilon|\rho)], \end{aligned} \quad (28a)$$

$$\begin{aligned} \psi_b &= kN' e^{i(j+\frac{1}{2})\theta} e^{i|\epsilon|\rho} \rho^{\nu-\frac{1}{2}} \\ &\times [j_1 F_1(\nu - \bar{Z}, 1 + 2\nu, -2i|\epsilon|\rho) - (\nu - \bar{Z}) \\ &\times {}_1F_1(1 + \nu - \bar{Z}, 1 + 2\nu, -2i|\epsilon|\rho)], \end{aligned} \quad (28b)$$

where  $\bar{Z} = iZ\alpha \text{sgn}(\epsilon)$ . We use the ZZBC by setting  $\psi_a(1, \theta) = 0$  or  $\psi_b(1, \theta) = 0$  for  $\delta = 0$ . The change  $\epsilon \rightarrow -\epsilon$  in Eqs. (28a) and (28b) results in different equations and shows that the electron-hole symmetry is broken, i.e.,

$$\epsilon_{\pm, i, m}^e \neq -\epsilon_{\pm, i, m}^h, \quad i = a, b. \quad (29)$$

Equations (28a) and (28b) can be transformed into one another by  $j \rightarrow -j$ ,

$$\epsilon_{\pm 1, a, j}^{e, h} = \epsilon_{\pm 1, b, -j}^{e, h}. \quad (30)$$

This indicates that having  $A$  or  $B$  sublattices at the edge of the QD changes the angular momentum label  $m$  while the whole spectrum remains invariant. This is the same as in the absence of a Coulomb impurity (see Ref. [16]) in which the

intervalley relationship

$$\epsilon_{+1,i,m}^{e,h} = \epsilon_{-1,i,-m}^{e,h}, \quad i = a, b \quad (31)$$

holds. It is readily seen that this relation is satisfied because  $j = km + 1/2$  and the changes  $k \rightarrow -k$  and  $m \rightarrow -m$  leave the equations invariant.

For  $\delta = 0$  we also consider the IMBC, Eq. (7). Applying it to Eqs. (28a) and (28b) leads to the following equation that determines the energy spectrum:

$$\begin{aligned} (1 \mp i\tau)j_1 F_1(v - \bar{Z}, 1 + 2v, -2i|\epsilon|) \\ - (1 \pm i\tau)(v - \bar{Z})_1 F_1(1 + v - \bar{Z}, 1 + 2v, -2i|\epsilon|) = 0; \end{aligned} \quad (32)$$

the combination  $(-, +)$  is used for  $\epsilon > \delta$  and  $(+, -)$  is used for  $\epsilon < \delta$ . The IMBC spectrum is invariant upon making the changes  $j \rightarrow -j$  and  $\tau \rightarrow -\tau$ . This corresponds to the intervalley relation Eq. (31) derived from the ZZBC.

In the limit  $\rho \rightarrow 0$ , the behavior of the wave functions (28a) and (28b) at the origin is given by

$$R_a(\rho) \sim R_b(\rho) \sim \rho^{v-1/2}. \quad (33)$$

But when  $v$  becomes imaginary, the factor  $\rho^{v-1/2}$  oscillates strongly, i.e.,  $e^{i|\nu|\ln(\rho)-1/2}$ , and the oscillation frequency increases as the origin is approached [10]. This makes the wave functions not normalizable. Thus, the problem of a Coulomb impurity is ill-defined in the supercritical regime  $Z\alpha > 1/2$ . The reason for that is the singularity of the Coulomb potential  $V(\rho) = -Z\alpha/\rho$  for  $\rho \rightarrow 0$ . This singularity can be removed by assuming a finite-size impurity.

#### IV. FINITE-SIZE IMPURITY: SUPERCRITICAL REGIME

As discussed above, the Dirac equation, with a pure Coulomb potential, can be solved in the subcritical regime,  $Z\alpha \leq 1/2$ , for all energy levels. For  $Z\alpha > 1/2$  we are in the supercritical regime. In this regime, the problem is ill-defined because of the singular behavior of the Coulomb potential at the origin. This singularity can be removed by putting the impurity above the graphene sheet or by taking into account the discrete nature of the graphene lattice. Here we assume that the impurity has a finite size  $r_0$ , which we take to be equal to the graphene lattice constant. This provides the extra boundary condition that is necessary for solving the problem. Explicitly, we assume the impurity potential

$$V(\rho) = \begin{cases} -Z\alpha/\rho_0, & \rho < \rho_0, \\ -Z\alpha/\rho, & \rho > \rho_0, \end{cases} \quad (34)$$

where  $\rho_0 = r_0/R$  (see Fig. 1). The Dirac equation will now be solved for  $\rho < \rho_0$  and  $\rho > \rho_0$  separately and the solutions will be matched at  $\rho = \rho_0$ . We take  $\rho_0 = a/R \ll 1$ , with  $a \approx 0.14$  nm the graphene lattice constant.

Inside the impurity, i.e., for  $\rho < \rho_0$ , we simply replace the term  $Z\alpha/\rho$  by  $Z\alpha/\rho_0$  in Eqs. (2a) and (2b). The corresponding solutions are the same as those in Sec. II A with  $\epsilon$  replaced by  $\epsilon + Z\alpha/\rho_0$ .

For  $\rho > \rho_0$ , we proceed as in Sec. III but with an important difference: we now include both solutions, the one that is regular at the origin and the one that is singular at it since the

origin is excluded. This latter solution was discarded in the subcritical regime.

The solutions for  $P(\rho)$  and  $Q(\rho)$  when  $|\epsilon| < \delta$  are

$$\begin{aligned} P(\rho) = A_1 F_1(v - \omega_\gamma, 1 + 2v, 2\gamma\rho) \\ + B(2\gamma\rho)^{-2v} {}_1F_1(-v - \omega_\gamma, 1 - 2v, 2\gamma\rho) \end{aligned} \quad (35a)$$

and

$$\begin{aligned} Q(\rho) = C_1 F_1(1 + v - \omega_\gamma, 1 + 2v, 2\gamma\rho) \\ + D(2\gamma\rho)^{-2v} {}_1F_1(1 - v - \omega_\gamma, 1 - 2v, 2\gamma\rho). \end{aligned} \quad (35b)$$

Note that  $v = [(km + 1/2)^2 - (Z\alpha)^2]^{1/2}$  is purely imaginary in the supercritical regime. We have *four* constants in Eqs. (35a) and (35b) that we can reduce to two by plugging the results back into the original equation; this gives the relations

$$\frac{C}{A} = \frac{v - \omega_\gamma}{j + \eta_\gamma}, \quad \frac{D}{B} = -\frac{v + \omega_\gamma}{j + \eta_\gamma}. \quad (36)$$

For the solutions in the region  $|\epsilon| > \delta$ , we simply make the substitution  $\gamma \rightarrow -i\beta$ ,  $\omega_\gamma \rightarrow i\omega_\beta$ , and  $\eta_\gamma \rightarrow i\eta_\beta$  in Eqs. (35a) and (35b).

In the gapless case ( $\delta = 0$ ), the equations outside the impurity are obtained by putting  $\omega_\beta = Z\alpha \operatorname{sgn}(\epsilon)$ ,  $\eta_\beta = 0$ , and  $\beta = |\epsilon|$  in the solutions for the  $|\epsilon| > \delta$  case [given by Eq. (35a) and (35b)].

For  $\rho > \rho_0$  we have two unknowns,  $A$  and  $B$ . Matching the wave functions at  $\rho_0$  gives the relations  $\psi_a^i = \psi_a^o$  and  $\psi_b^i = \psi_b^o$ , where  $i$  ( $o$ ) label the solutions inside (outside) the impurity. This leads to

$$\frac{\psi_a^i}{\psi_b^i} = \frac{\psi_a^o}{\psi_b^o}, \quad (37)$$

and, together with Eq. (36), it relates  $A$  to  $B$ . Inside the impurity, the solutions are

$$\begin{aligned} \psi_a^i(\rho, \theta) = e^{im\theta} J_m[(\epsilon + Z\alpha/\rho_0)\rho], \\ \psi_b^i(\rho, \theta) = i e^{i(m+k)\theta} J_{m+k}[(\epsilon + Z\alpha/\rho_0)\rho]. \end{aligned} \quad (38)$$

Now we will use Eq. (37), the fact that the impurity size is very small,  $\rho_0 \ll 1$ , and the approximation  ${}_1F_1(a, b, z) \approx 1$ ,  $z \ll 1$ , for  $\rho > \rho_0$ . Then  $P$  and  $Q$  take the simpler form

$$P(\rho) = j[A + B(-2i|\epsilon|\rho)^{-2v}], \quad (39a)$$

$$Q(\rho) = A(v - \bar{Z}) + B(-v - \bar{Z})(-2i|\epsilon|\rho)^{-2v}. \quad (39b)$$

Then matching at  $\rho_0$  gives

$$\frac{B}{A} = (-2i|\epsilon|\rho_0)^{2v} \frac{(C_1 k - C_2)j - (C_1 k + C_2)(v - \bar{Z})}{(C_2 - C_1 k)j + (C_1 k + C_2)(-v - \bar{Z})}, \quad (40)$$

where  $C_1 = \pm J_m[(\epsilon + Z\alpha/\rho_0)\rho_0]$  and  $C_2 = i J_{m+k}[(\epsilon + Z\alpha/\rho_0)\rho_0]$ .

For  $\delta \neq 0$  the relation between  $A$  and  $B$  can be obtained in a completely analogous way. Outside the impurity we need to consider two cases:  $|\epsilon| > \delta$  and  $|\epsilon| < \delta$ . For the solutions inside the impurity, in principle, there are also two cases to consider:  $|\epsilon + Z\alpha/\rho_0| > \delta$  and  $|\epsilon + Z\alpha/\rho_0| < \delta$ . But the size

of the impurity  $\rho_0$  is very small compared to that of the dot because  $Z\alpha/\rho_0$  is very large. Thus inside the impurity we only need to look at the case  $\epsilon + Z\alpha/\rho_0 > \delta$ . For  $|\epsilon| < \delta$ , we obtain

$$\frac{B}{A} = (2\gamma\rho_0)^{2\nu} \frac{(D_1k - D_2)(j + \eta_\gamma) - (D_1k + D_2)(v - \omega_\gamma)}{(D_2 - D_1k)(j + \eta_\gamma) - (D_1k + D_2)(v + \omega_\gamma)}, \quad (41)$$

where  $D_1 = \sqrt{|\epsilon - \delta|} J_m [(\epsilon + Z\alpha/\rho_0)^2 - \delta^2]^{1/2} \rho_0$  and  $D_2 = \sqrt{|\epsilon + \delta|} J_{m+k} [(\epsilon + Z\alpha/\rho_0)^2 - \delta^2]^{1/2} \rho_0$ .

In the range  $|\epsilon| > \delta$ , the ratio  $B/A$  is obtained after the substitutions  $\gamma \rightarrow -i\beta$ ,  $\omega_\gamma \rightarrow i\omega_\beta$ ,  $\eta_\gamma \rightarrow i\eta_\beta$ ,  $D_1 \rightarrow \pm D_1$  (where the + sign is for  $\epsilon > \delta$  and the - sign is for  $\epsilon < -\delta$ ), and  $D_2 \rightarrow iD_2$  in Eq. (41). Having determined all constants, we can impose the IMBC and ZZBC at the edge of the dot.

(i) ZZBC,  $\delta = 0$ . We apply the ZZBC  $\psi_a(1, \theta) = 0$  [note that  $\psi_a(1, \theta) = 0$  and  $\psi_b(1, \theta) = 0$  give the same results].  $\psi_a$  is obtained by inserting Eqs. (35a) and (35b) in Eq. (19). Then using Eq. (40) we obtain the spectrum in the subcritical and supercritical regime by finding the zeros of the equation

$$\begin{aligned} & j[{}_1F_1(v - \bar{Z}, 1 + 2\nu, -2i|\epsilon|) \\ & + \mathcal{B}{}_1F_1(-v - \bar{Z}, 1 - 2\nu, -2i|\epsilon|)] \\ & + (v - \bar{Z}){}_1F_1(1 + v - \bar{Z}, 1 + 2\nu, -2i|\epsilon|) \\ & + \mathcal{B}(-v - \bar{Z}){}_1F_1(1 - v - \bar{Z}, 1 - 2\nu, -2i|\epsilon|) = 0, \end{aligned} \quad (42)$$

where  $\mathcal{B}$  is given by

$$\mathcal{B} = -\rho_0^{2\nu} \frac{(C_1k - C_2)j - (C_1k + C_2)(v - \bar{Z})}{(C_1k - C_2)j + (C_1k + C_2)(v + \bar{Z})}. \quad (43)$$

In the subcritical regime ( $Z\alpha < 1/2$ ),  $\nu$  is real for all  $m$  values, and since  $\rho_0$  is very small,  $\mathcal{B}$  will also be very small. Because of this, Eq. (42) will reduce to that for a point-size nucleus, Eq. (25a), with  $\delta = 0$ .

(ii) IMBC,  $\delta = 0$ . As stated before, we will consider only gapless graphene. Using the wave functions Eqs. (35a) and (35b) and imposing the IMBC leads to the equation

$$\begin{aligned} & (1 \mp i\tau)j[{}_1F_1(v - \bar{Z}, 1 + 2\nu, -2i|\epsilon|) \\ & + \mathcal{B}{}_1F_1(-v - \bar{Z}, 1 - 2\nu, -2i|\epsilon|)] \\ & - (v - \bar{Z})(1 \pm i\tau){}_1F_1(1 + v - \bar{Z}, 1 + 2\nu, -2i|\epsilon|) \\ & = -(v + \bar{Z})(1 \pm i\tau)\mathcal{B}{}_1F_1(1 - v - \bar{Z}, 1 - 2\nu, -2i|\epsilon|). \end{aligned} \quad (44)$$

$\mathcal{B}$  is again given by Eq. (43). It is readily seen that Eq. (44) reduces to Eq. (32) in the subcritical regime because  $\nu$  becomes real and  $\rho_0 \ll 1$ .

The solutions of Eqs. (42) and (44) result in real energies. However, in the limit of  $R \rightarrow \infty$ , i.e., the case of a graphene sheet,  $\rho_0 = r_0/R \rightarrow 0$  and  $\mathcal{B} \rightarrow 0$  and these solutions give complex energies.

(iii) ZZBC,  $\delta \neq 0$ . For  $|\epsilon| < \delta$  we use the wave functions Eqs. (35a), (35b), and (41). With this and  $\psi_a(1, \theta) = 0$  we get

$$\begin{aligned} & (j + \eta_\gamma)[{}_1F_1(v - \omega_\gamma, 1 + 2\nu, 2\gamma) \\ & + \mathcal{D}{}_1F_1(-v - \omega_\gamma, 1 - 2\nu, 2\gamma)] \\ & + (v - \omega_\gamma){}_1F_1(1 + v - \omega_\gamma, 1 + 2\nu, 2\gamma) \\ & + \mathcal{D}(-v - \omega_\gamma){}_1F_1(1 - v - \omega_\gamma, 1 - 2\nu, 2\gamma) = 0. \end{aligned} \quad (45)$$

If we set  $\psi_b(1, \theta) = 0$ , we obtain Eq. (45) with the opposite sign at the start of the last two lines. In both cases,  $\mathcal{D}$  is given by

$$\mathcal{D} = -\rho_0^{2\nu} \frac{(D_1k - D_2)(j + \eta_\gamma) - (D_2 + D_1k)(v - \omega_\gamma)}{(D_1k - D_2)(j + \eta_\gamma) + (D_2 + D_1k)(v + \omega_\gamma)}. \quad (46)$$

The results for  $|\epsilon| > \delta$  can be obtained by making the changes  $\gamma \rightarrow -i\beta$ ,  $\omega_\gamma \rightarrow i\omega_\beta$ ,  $\eta_\gamma \rightarrow i\eta_\beta$ ,  $D_1 \rightarrow \pm D_1$  (where the + sign is for  $\epsilon > \delta$  and the - sign is for  $\epsilon < -\delta$ ), and  $D_2 \rightarrow iD_2$  in Eqs. (45) and (46).

## V. NUMERICAL RESULTS

Below we present the results obtained by numerically solving the different equations determining the energy spectra given in Secs. III and IV.

### A. Zigzag boundary conditions

Figure 3(a) shows the spectrum as a function of the impurity strength  $Z\alpha$  for a QD with ZZBC and  $\delta = 0$  for the three angular momentum labels  $m = 0, 1, -1$ . The dashed curves are for a point-size impurity and the solid ones for a finite-size impurity. The dot radius is  $R = 70$  nm and that of the finite-size impurity  $r_0$  is taken equal to the graphene lattice constant  $\rho_0 = 0.142$  nm. The vertical gray line at  $Z\alpha = 0.5$  marks the critical impurity strength  $Z\alpha = 1/2$ , i.e., the value for  $m = 0, -1$ , at which the supercritical regime starts. The spectrum is plotted only for the  $K$  valley since valley symmetry is preserved in the presence of the impurity. If there is no impurity, the energy spectrum exhibits degenerate zero-energy states for the quantum numbers  $m < 0$  (for  $k = 1$ ). These states are the *edge states* brought about by the ZZBC. To study the dependence of the edge states on the impurity strength, we show in Fig. 3(b) the edge states corresponding to all angular momentum labels. As  $Z\alpha$  increases, they are pulled downward by the impurity, almost forming an energy band, and the ones with the highest  $m$  allowed always remain below the line  $\epsilon = -Z\alpha$  in both the subcritical and supercritical regimes. This is proven analytically in the Appendix by substituting  $\epsilon = -Z\alpha$  in Eq. (28a) and verifying that  $\psi_a(1, \theta) = 0$  in the limit  $j \rightarrow -\infty$ . As the impurity strength increases, the states that enter the supercritical regime ( $Z\alpha > |km + 1/2|$ ) start to detach themselves from the band rather abruptly. We note that the zero-energy level corresponds to the Fermi energy  $E_F$  when the charge in the system is zero. Adding the charge  $Z\alpha$  to the system makes  $E_F$  move as  $E_F = -Z\alpha$  to preserve its charge neutrality. In the inset of Fig. 3(b) we have compared the probability densities corresponding to the edge state with  $m = -2$  in the subcritical regime ( $Z\alpha = 1$ ) with that in the supercritical regime (with  $Z\alpha = 1.7$ ). One can see that the edge state is not very affected by the impurity subcritical regime and therefore is more localized at the edge of the dot. However, in the supercritical regime the probability density exhibits a sharp peak around the impurity, changing the edge state into an impurity state.

The point-size impurity gives sensible solutions only for  $Z\alpha < |km + 1/2|$  (subcritical regime), which coincide with those obtained using a finite size-impurity. The latter model gives solutions in both the subcritical and supercritical

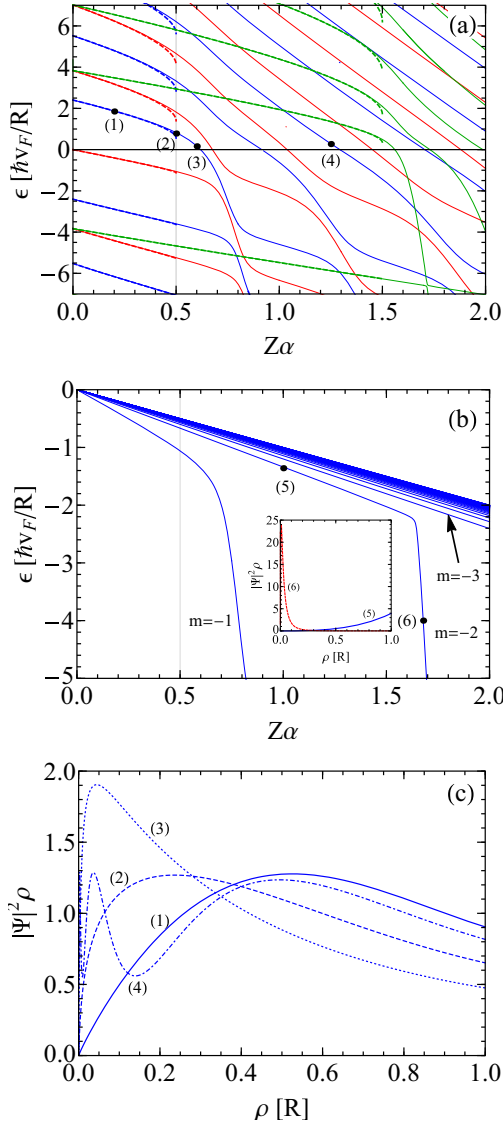


FIG. 3. (a) Energy spectrum for a dot, of radius  $R = 70$  nm, with a Coulomb impurity and the ZZBC, vs its strength  $Z\alpha$  (the spectrum is symmetric with respect to the  $K$  and  $K'$  valleys). The dashed curves are for a point impurity and the solid ones for a finite-size impurity of radius equal to the lattice parameter ( $\rho_0 = 0.142$  nm). The angular momentum numbers are  $m = 0$  (blue),  $m = 1$  (green), and  $m = -1$  (red). (b) The edge states that start at  $\epsilon = 0$  vs the strength  $Z\alpha$ . The ones with the highest  $m$  allowed always remain below the line  $\epsilon = -Z\alpha$ . In the inset the probability density at the points (5) and (6) is shown. (c) Probability density vs  $\rho$  for the points labeled by (1)–(4) in (a).

regimes. As we enter the supercritical ( $Z\alpha > |km + 1/2|$ ) regime (e.g.,  $Z\alpha > 1/2$  for  $m = 0, -1$  and  $Z\alpha > 3/2$  for  $m = 1, -2$ ), the energy levels start to display atomic collapse: (i) for each  $m$  the lowest electron state turns into a hole state, and (ii) the spectrum shows anticrossings between the energy levels with the same  $m$  resulting from the oscillating wave functions in the supercritical regime. In Fig. 3(c) we show the probability densities corresponding to the energies labeled by (1)–(4) in the spectrum of Fig. 3(a). When the strength  $Z\alpha$

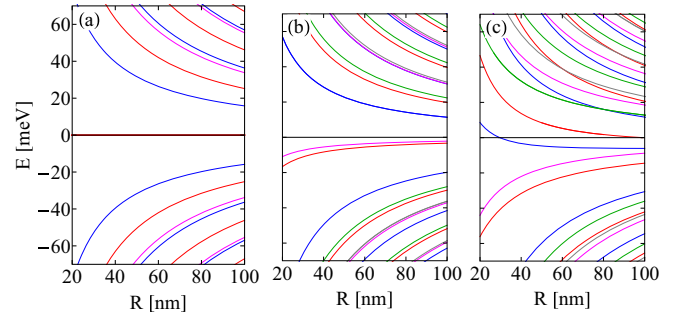


FIG. 4. Energy levels as functions of the dot radius  $R$  for the ZZBC with  $m = 0$  (blue),  $m = 1$  (green),  $m = -1$  (red),  $m = 2$  (gray), and  $m = -2$  (magenta). The value of  $Z\alpha$  is 0 in (a), 0.25 in (b), and 1 in (c).

increases, the electron gets closer to the impurity and its wave function exhibits oscillatory behavior; see curves (3) and (4). The fact that the electron comes closer to the impurity is a typical sign of atomic collapse.

In Fig. 4 the dependence on the dot radius  $R$  of the  $m = 0, \pm 1, \pm 2$  states is shown. In the absence of impurity, Fig. 4(a), the energy levels exhibit a  $1/R$  dependence. This dependency holds in the subcritical regime [e.g., Fig. 4(b) for  $Z\alpha = 0.25$ ] for both the bulk and those of the edges states with  $m = -1, -2$ , which are separated from the zero-energy levels in the case of  $Z\alpha = 0$ ; see the discussion for Fig. 2(b). In the supercritical regime, Fig. 4(c), the states start to deviate from the  $1/R$  behavior. To better understand the size dependence of the energy levels in Figs. 5(a) and 5(b), we follow the  $R$  dependence of the lowest electron states (in the subcritical regime) with  $m = 0$  and 1, respectively, for different  $Z\alpha$  from the subcritical to the supercritical regime [the states labeled by (1)–(4) in Fig. 3(a)]. The results are shown in Fig. 5(a). We find that the energy levels show a  $1/R$  dependence in the supercritical regime (note that energies are plotted in units of  $\hbar v_F/R$ ). The red curve is for  $Z\alpha = 1/2$  and marks the boundary between the subcritical and supercritical regime. In the supercritical regime  $Z\alpha > 1/2$ , the  $1/R$  dependence

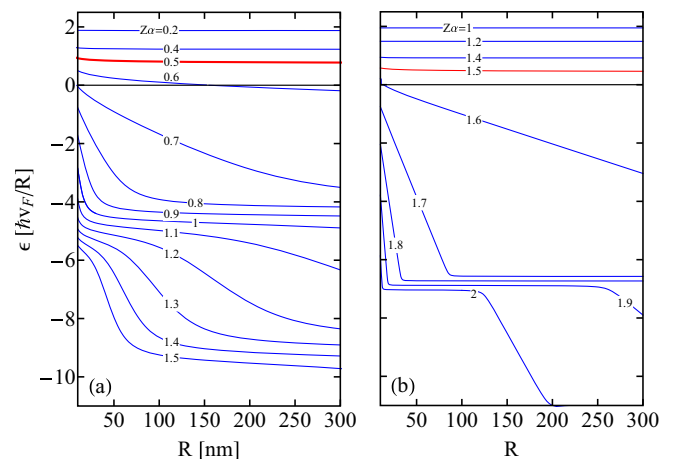


FIG. 5. (a) The lowest  $m = 0$  electron state (in subcritical regime) as a function of  $R$  for different  $Z\alpha$  from the subcritical to supercritical regime. (b) The same as in (a) but now for  $m = 1$ .

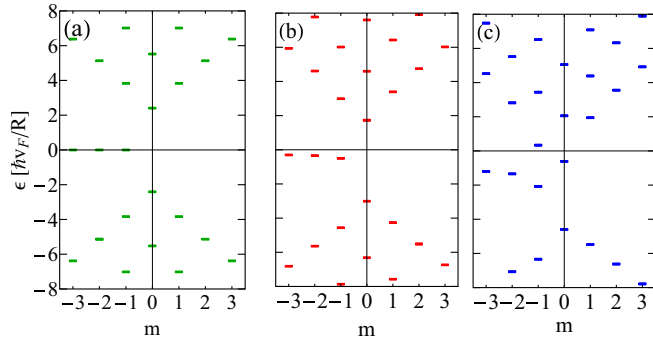


FIG. 6. Energy levels as functions of the angular momentum number  $m$  for a dot with the ZZBC and  $R = 70$  nm. The impurity strength  $Z\alpha$  is 0 in (a), 0.25 in (b), and 1 in (c).

breaks down and the levels decrease nonmonotonically as a function of  $R$ . This can be explained from Eq. (43), which contains the factor  $\rho_0^{2\nu}$  with  $\nu$  imaginary for  $Z\alpha > |km + 1/2|$ , and it results in an oscillating function. In Fig. 5(b), we follow the lowest electron state (at  $Z\alpha = 0$ ) with  $m = 1$  from the subcritical to the supercritical regime, and we show its  $R$  dependence for different  $Z\alpha$  values. The lowest  $m = 1$  state enters into the supercritical regime when  $Z\alpha > 3/2$ . Although in the subcritical regime ( $Z\alpha < 3/2$ ) the levels exhibit a  $1/R$  dependence, i.e., the same as Fig. 5(a), in the supercritical regime the levels decrease with  $R$  more abruptly compared to the case of  $m = 0$ . This can be linked to the larger strength of the Coulomb interaction in the supercritical regime compared to the  $m = 0$  state, where we enter into the supercritical regime for  $Z\alpha > 1/2$ .

In Fig. 6, the dependence of the levels on the angular momentum label  $m$  is shown for a QD with  $R = 70$  nm and  $Z\alpha = 0, 0.25, 1$ . Due to the ZZBC, the energy levels for  $m \neq 0$ , except the zero energy levels, are doubly degenerate,  $\epsilon_m^{e,h} = \epsilon_{-m}^{e,h}$  for  $Z\alpha = 0$  [see Fig. 6(a)]. This degeneracy is broken by the impurity, and the resulting spectrum depends more strongly on  $m$  as the impurity strength increases; see Figs. 6(b) and 6(c). As  $Z\alpha$  increases, the degeneracy of the edge states (with  $m < 0$ ) is partially lifted, starting from the lowest  $m$  states, while the other levels remain degenerate with  $\epsilon = -Z\alpha$ . Once an edge state enters the supercritical regime, it deviates sharply from the other edge states (notice the energy of the  $m = -1$  state at  $Z\alpha = 0.25 < 1/2$  and  $Z\alpha = 1 > 1/2$ ).

In Fig. 7, we show the dependence of the energy levels of a QD with a ZZBC, obtained from  $\psi_a(1, \theta) = 0$ , in the presence of the induced mass potential  $\delta$ . When no charge is present, none of the states will dive below the gap line ( $\epsilon = \delta$ ). Adding an impurity will cause some states to be pushed inside the gap, and increasing its strength will push more levels inside it. Unlike the case  $\delta = 0$ , in which the electron states enter the holes' space only in the supercritical regime, for  $\delta \neq 0$  electron states are pushed into the gap even in the subcritical regime; see Fig. 7(b), where the lowest  $m = 0$  state enters the gap at  $\delta \gtrsim 3$ . For large  $\delta$ , the levels depend nearly linearly on the gap. The edge states for  $\delta \neq 0$  have now the energy  $\epsilon = -\delta$ , they are pulled downward by the impurity, and they remain below the line  $\epsilon = -\delta - Z\alpha$ .

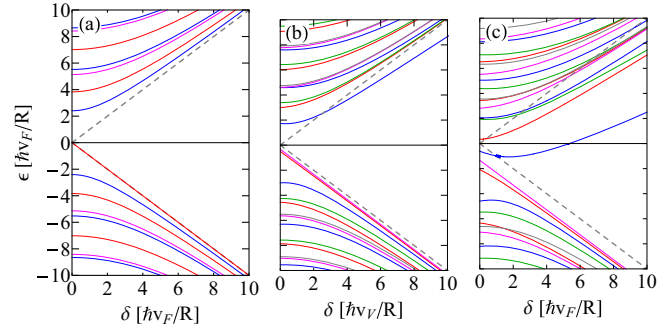


FIG. 7. Energy levels vs the mass potential term  $\delta$  for the ZZBC. The impurity strength  $Z\alpha$  is 0 in (a), 0.25 in (b), and 1 in (c). The color code is that of Fig. 4.

### B. Infinite-mass boundary conditions

Here we present the results for a circular graphene QD with the IMBC given by Eq. (7). The spectrum as a function of the impurity size ( $Z\alpha$ ) is shown in Fig. 8(a) for angular momentum numbers  $m = 0, 1, -1$ . The spectrum is obtained using the point-size (in the subcritical regime) and finite-size nucleus (in both subcritical and supercritical regimes). Unlike the ZZBC, with an IMBC there are no zero-energy states (edge states) in the spectrum. Similar to our results

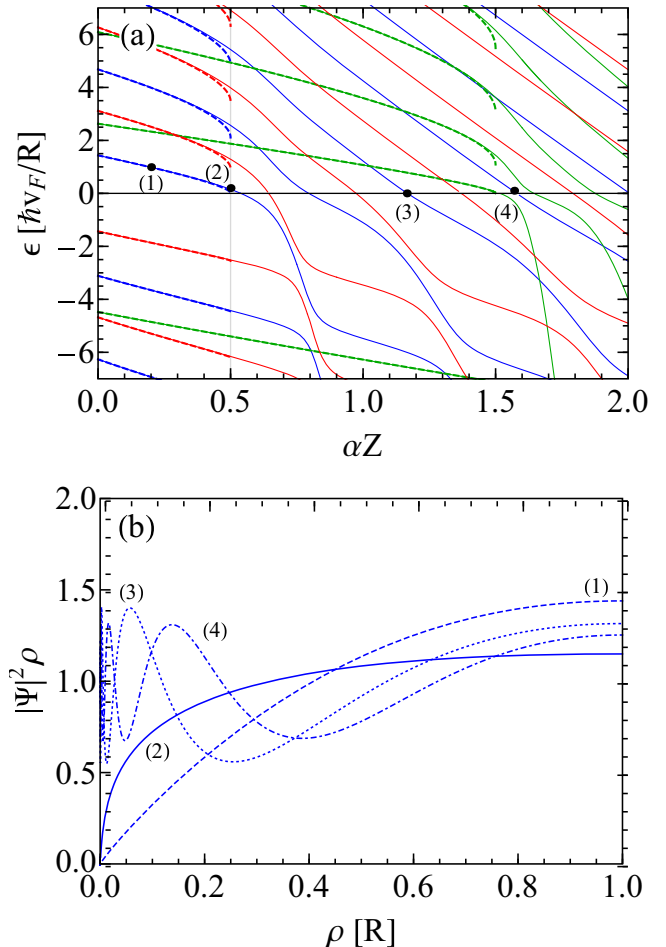


FIG. 8. The same as Fig. 3 but now with the IMBC.

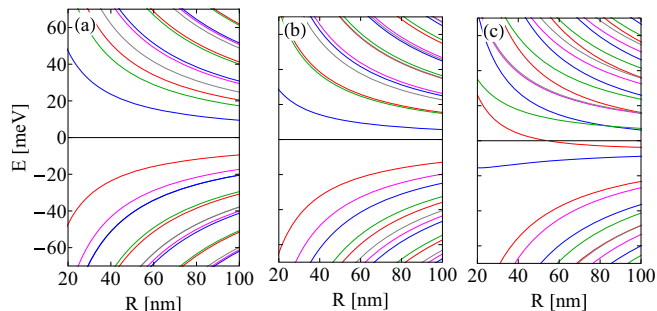


FIG. 9. The same as Fig. 4 but now with the IMBC.

for QDs with ZZBC, both point-size and finite-size models agree quite well in the subcritical regime. Figure 8(b) shows the probability densities corresponding to the energy points labeled by (1)–(4) in Fig. 8(a). In the supercritical regime, there are again oscillations, as in the ZZBC case, that increase in frequency with increasing charge, and the electrons are pushed closer to the impurity. The wave functions (35) contain the factor  $\rho^{-2i\sqrt{(Z\alpha)^2 - j^2}}$  in the supercritical regime, which can be rewritten as  $e^{-2i\sqrt{(Z\alpha)^2 - j^2} \log \rho}$ . This indicates that the wave functions oscillate more around the impurity ( $\rho = 0$ ) when the charge is increased, as shown in Fig. 8(b). Comparing the spectrum of the ZZBC [Fig. 3(a)] to that of the IMBC [Fig. 8(a)], one can see that both spectra start to resemble each other when the strength of the impurity increases because when the electrons get closer to the impurity, the influence of the edges is weakened.

The energy levels as a function of the dot radius  $R$  are shown in Fig. 9 for the IMBC and for  $Z\alpha = 0, 0.25, 0.5$  in panels (a), (b), and (c), respectively. The plots are for  $|m| \leq 2$ . In contrast to the ZZBC, there is no zero-energy level in the absence of the impurity, and the spectrum shows different symmetries with respect to the angular momentum when the impurity is present. However, the overall  $R$  dependence of the energy levels is similar to that for the ZZBC (see Fig. 9): In the subcritical regime, the levels exhibit a  $1/R$  dependence and start to deviate from this in the supercritical regime decreasing nonmonotonically as a function of  $R$ . The overall behavior is the same as in the case of the ZZBC shown in Fig. 5.

The angular dependence of the energy levels is shown in Fig. 10. The IMBC implies different symmetries from those for the ZZBC. The symmetries  $\epsilon_m^{e(h)} = \epsilon_{-m}^{e(h)}$  and  $\epsilon_m^e = -\epsilon_m^h$ , for the levels with  $\epsilon \neq 0$ , are no longer present in the IMBC spectrum

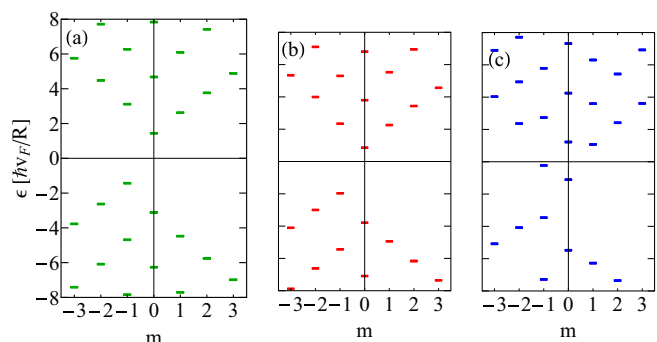


FIG. 10. The same as Fig. 4 but now with the IMBC.

without impurity. However, the energy levels display the symmetry  $\epsilon_m^e = \epsilon_{-(m+1)}^h$ ,  $m \neq 0$  [Eq. (15a)], which is broken by the impurity. The lowest electron state in the subcritical regime is for  $m = 0$  for both ZZBC and IMBC. However, the lowest hole state of the dot with IMBC is for  $m = -1$  and for the ZZBC it is associated with the degenerate  $\epsilon_{m < 0}^h = -Z\alpha$  states.

## VI. SUMMARY

We studied the problem of a Coulomb charge at the center of a circular graphene QD with a ZZBC or IMBC. Within a continuum approach, we considered both a point-size and a finite-size impurity, obtained analytical expressions for the wave functions, and derived expressions for the energies. The main difference between the system of a charged impurity in a graphene QD and in bulk graphene is that in bulk graphene the atomic collapse manifests itself as resonances associated with the *quasibound states* (having a finite lifetime), while in a QD an impurity can only influence the *localized bound states* due to confinement. Due to the confinement of carriers in a finite-size QD, we found discrete real energy states in both the subcritical ( $Z\alpha < |km + 1/2|$ ) and supercritical ( $Z\alpha > |km + 1/2|$ ) regimes, with  $k = \pm 1$  distinguishing the  $K$  and  $K'$  valleys and  $m$  the angular momentum label. This is in contrast with the case of a Coulomb impurity in a bulk graphene sheet where the eigenvalues are complex in the supercritical regime. However, we found that the wave functions start to oscillate near the Coulomb impurity in the supercritical regime, indicating atomic collapse in graphene QDs. In this regime, the lowest electron state for each  $m$  turns into a hole state, and the spectrum shows anticrossings between the energy levels. In the presence of a mass term  $\delta$ , the lowest electron states can enter into the gap as  $\delta$  increases even in the subcritical regime.

We showed that the degeneracy of the edge states, with  $\epsilon = 0$ , for QDs with the ZZBC is lifted by the impurity, the states almost form an energy band, and the ones with the highest allowed  $m$  always remain below the line  $\epsilon = -Z\alpha$ . While in the presence of an impurity the valley symmetry is preserved, we find that the impurity breaks electron-hole symmetry. We further demonstrated that the energy levels have a  $1/R$  dependence in the subcritical regime. This dependence no longer exists in the supercritical regime, and the levels decrease as a function of  $R$  in a nonmonotonic manner, showing the signature of atomic collapse in graphene QDs.

## ACKNOWLEDGMENTS

We thank Massoud Ramezani-Masir and Dean Moldovan for fruitful discussions. This work was supported by the Flemish Science Foundation (FWO-VI), the Methusalem funding of the Flemish Government, and by the Canadian NSERC Grant No. OGP0121756 (P.V.).

## APPENDIX

We start with Eq. (28a) and look at  $\psi_a(1, \theta) = 0$  when  $\epsilon = -Z\alpha$  and check if the equation is satisfied in the limit  $j \rightarrow -\infty$ . In the limit  $j \rightarrow -\infty$ , we can replace  $\nu = \sqrt{j^2 - (Z\alpha)^2}$

by  $|j|$  in Eq. (28a). With  $\tilde{Z} = i|Z\alpha|$ , this gives

$$-|j| {}_1F_1(|j| + \tilde{Z}, 1 + 2|j|, -2\tilde{Z}) + (|j| + \tilde{Z}) {}_1F_1(1 + |j| + \tilde{Z}, 1 + 2|j|, -2\tilde{Z}) = 0. \quad (\text{A1})$$

Using the relation  ${}_1F_1(a, b, z) - {}_1F_1(a - 1, b, z) = (z/b) {}_1F_1(a, b + 1, z)$ , we can rewrite the terms with the prefactor  $|j|$  of Eq. (A1) as

$$- [|j|/(1 + 2|j|)] \tilde{Z} {}_1F_1(1 + |j| + \tilde{Z}, 2 + 2|j|, -2\tilde{Z}). \quad (\text{A2})$$

Putting this result back in Eq. (A1), we have

$$[\tilde{Z} {}_1F_1(1 + \tilde{Z} + |j|, 1 + 2|j|, -2\tilde{Z}) - [|j|/(1 + 2|j|)] \times 2\tilde{Z} {}_1F_1(1 + \tilde{Z} + |j|, 2 + 2|j|, -2\tilde{Z})] = 0. \quad (\text{A3})$$

Using the series expansion  ${}_1F_1(a, b, z) = 1 + (a/b)z + [a(a + 1)/b(b + 1)2!]z^2 + \dots$ , the confluent hypergeometric

functions in Eq. (A3) can be written as

$$\begin{aligned} & {}_1F_1(1 + \tilde{Z} + |j|, 1 + 2|j|, -2\tilde{Z}) \\ &= 1 - \frac{(1 + \tilde{Z} + |j|)}{1 + 2|j|} \\ & \times \left[ 2\tilde{Z} - \frac{(1 + \tilde{Z} + |j|)(2 + \tilde{Z} + |j|)4\tilde{Z}^2}{(2 + 2|j|)2!} + \dots \right], \end{aligned} \quad (\text{A4})$$

and in the limit  $j \rightarrow -\infty$  they simplify to

$$\begin{aligned} & {}_1F_1(1 + \tilde{Z} + |j|, 1 + 2|j|, -2\tilde{Z}) \\ &= 1 - \tilde{Z} + \tilde{Z}^2/2! - \tilde{Z}^3/3! + \dots = e^{-\tilde{Z}}. \end{aligned} \quad (\text{A5})$$

Now inserting  ${}_1F_1 = e^{-\tilde{Z}}$  in Eq. (A3) and considering  $|j|/(1 + 2|j|) \rightarrow 1/2$ , one can see that in the limit  $j \rightarrow -\infty$  the left side of Eq. (A3) vanishes.

- 
- [1] W. Greiner, B. Müller, and J. Rafelski, *Quantum Electrodynamics of Strong Fields* (Springer, Berlin, 1985).
- [2] I. Pomeranchuk and Y. Smorodinsky, *Sov. Phys. USSR* **9**, 97 (1945).
- [3] Y. Zeldovich and V. S. Popov, *Sov. Phys. Usp.* **14**, 673 (1972).
- [4] T. Cowan, H. Backe, M. Begemann, K. Bethge, H. Bokemeyer, H. Folger, J. S. Greenberg, H. Grein, A. Gruppe, Y. Kido, M. Klüver, D. Schwalm, J. Schweppe, K. E. Stiebing, N. Trautmann, and P. Vincent, *Phys. Rev. Lett.* **54**, 1761 (1985).
- [5] A. V. Shytov, M. I. Katsnelson, and L. S. Levitov, *Phys. Rev. Lett.* **99**, 236801 (2007).
- [6] O. O. Sobol, E. V. Gorbar, and V. P. Gusynin, *Phys. Rev. B* **88**, 205116 (2013).
- [7] V. M. Pereira, J. Nilsson, and A. H. C. Neto, *Phys. Rev. Lett.* **99**, 166802 (2007).
- [8] Y. Wang, D. Wong, A. V. Shytov, V. W. Brar, S. Choi, Q. Wu, H.-Z. Tsai, W. Regan, A. Zettl, R. K. Kawakami, S. G. Louie, L. S. Levitov, and M. F. Crommie, *Science* **340**, 734 (2013).
- [9] J. Mao, Y. Jiang, D. Moldovan, G. Li, K. Watanabe, T. Taniguchi, M. R. Masir, F. M. Peeters, and E. Y. Andrei, *Nat. Phys.* **12**, 545 (2016).
- [10] D. Moldovan, Ph.D. thesis, University of Antwerp (2016).
- [11] A. V. Rozhkov, G. Giavaras, Y. P. Bliokh, V. Freilikher, and F. Nori, *Phys. Rep.* **503**, 77 (2011).
- [12] W.-d. Sheng, M. Korkusinski, A. D. Güçlü, M. Zielinski, P. Potasz, E. S. Kadantsev, O. Voznyy, and P. Hawrylak, *Front. Phys.* **7**, 328 (2012).
- [13] F. Molitor, J. Güttinger, C. Stampfer, S. Dröscher, A. Jacobsen, T. Ihn, and K. Ensslin, *J. Phys.: Condens. Matter* **23**, 243201 (2011).
- [14] S. Schnez, K. Ensslin, M. Sigrist, and T. Ihn, *Phys. Rev. B* **78**, 195427 (2008).
- [15] Z. Z. Zhang, K. Chang, and F. M. Peeters, *Phys. Rev. B* **77**, 235411 (2008).
- [16] M. Grujić, M. Zarenia, A. Chaves, M. Tadić, G. A. Farias, and F. M. Peeters, *Phys. Rev. B* **84**, 205441 (2011).
- [17] M. Zarenia, A. Chaves, G. A. Farias, and F. M. Peeters, *Phys. Rev. B* **84**, 245403 (2011).
- [18] H. P. Heiskanen, M. Manninen, and J. Akola, *New J. Phys.* **10**, 103015 (2008).
- [19] M. V. Berry and R. J. Mondragon, *Proc. R. Soc. London, Ser. A* **412**, 53 (1987).
- [20] G. Giovannetti, P. A. Khomyakov, G. Brocks, P. J. Kelly, and J. van den Brink, *Phys. Rev. B* **76**, 073103 (2007).
- [21] S. Y. Zhou, G.-H. Gweon, A. V. Fedorov, P. N. First, W. A. de Heer, D.-H. Lee, F. Guinea, A. H. C. Neto, and A. Lanzara, *Nat. Mater.* **6**, 770 (2007).
- [22] R. Quhe, J. Zheng, G. Luo, Q. Liu, R. Qin, J. Zhou, D. Yu, S. Nagase, W.-N. Mei, Z. Gao, and J. Lu, *NPG Asia Mater.* **4**, e6 (2012).
- [23] A. R. Akhmerov and C. W. J. Beenakker, *Phys. Rev. B* **77**, 085423 (2008).
- [24] I. S. Gradshteyn and I. M. Ryzhik, *Tables of Integrals, Series and Products* (Academic, New York, 1980), p. 803.
- [25] K. S. Gupta and S. Sen, *Phys. Rev. B* **78**, 205429 (2008).
- [26] D. S. Novikov, *Phys. Rev. B* **76**, 245435 (2007).